Intracluster age gradients in numerous young stellar clusters

K. V. Getman,[1]⋆ E. D. Feigelson,[1] M. A. Kuhn,[2,3] M. R. Bate,[4] P. S. Broos[1] and G. P. Garmire[5]

[1]*Department of Astronomy and Astrophysics, 525 Davey Laboratory, Pennsylvania State University, University Park, PA 16802, USA*
[2]*Instituto de Fisica y Astronomia, Universidad de Valparaiso, Gran Bretana 1111, Playa Ancha, Valparaiso, Chile*
[3]*Millenium Institute of Astrophysics, Av. Vicuna Mackenna 4860, 782-0436 Macul, Santiago, Chile*
[4]*Department of Physics and Astronomy, University of Exeter, Stocker Road, Devon, Exeter EX4 4QL, UK*
[5]*Huntingdon Institute for X-ray Astronomy, LLC, 10677 Franks Road, Huntingdon, PA 16652, USA*

ABSTRACT

The pace and pattern of star formation leading to rich young stellar clusters is quite uncertain. In this context, we analyse the spatial distribution of ages within 19 young (median $t \lesssim 3$ Myr on the Siess et al. time-scale), morphologically simple, isolated, and relatively rich stellar clusters. Our analysis is based on young stellar object (YSO) samples from the Massive Young Star-Forming Complex Study in Infrared and X-ray and Star Formation in Nearby Clouds surveys, and a new estimator of pre-main sequence (PMS) stellar ages, Age_{JX}, derived from X-ray and near-infrared photometric data. Median cluster ages are computed within four annular subregions of the clusters. We confirm and extend the earlier result of Getman et al. (2014): 80 per cent of the clusters show age trends where stars in cluster cores are younger than in outer regions. Our cluster stacking analyses establish the existence of an age gradient to high statistical significance in several ways. Time-scales vary with the choice of PMS evolutionary model; the inferred median age gradient across the studied clusters ranges from 0.75 to 1.5 Myr pc^{-1}. The empirical finding reported in the present study – late or continuing formation of stars in the cores of star clusters with older stars dispersed in the outer regions – has a strong foundation with other observational studies and with the astrophysical models like the global hierarchical collapse model of Vázquez-Semadeni et al.

Key words: stars: early-type – stars: formation – stars: pre-main sequence – open clusters and associations: general – infrared: stars – X-rays: stars.

1 INTRODUCTION

Although it is recognized that most stars in the Galaxy form today in clusters with 10^2–10^4 stars (Lada & Lada 2003), the pace and pattern of star formation leading to rich stellar clusters is quite uncertain. It is unclear whether clusters form rapidly in a burst of star formation of a large and dense molecular core (Elmegreen 2000), or over millions of years in filamentary concentrations of a turbulent molecular cloud (Krumholz & Tan 2007).

Observationally, comparison of individual cluster members and evolutionary tracks on a Hertzsprung–Russell diagram (HRD) typically shows a wide age dispersion, but this is difficult to interpret due to various observational and theoretical reasons such as photometric variability, multiplicity, and accretion history (Preibisch 2012). The situation is confused by the presence of mass segregation in some clusters, which may or may not arise from a delayed forma-

tion process for massive OB stars (Zinnecker & Yorke 2007). These issues are debated even for the most well-studied case, where the full stellar population is identified, the Orion nebula cluster (ONC; Hillenbrand 1997; Huff & Stahler 2006; O'Dell et al. 2009; Jeffries et al. 2011; Reggiani et al. 2011; Da Rio et al. 2014; Beccari et al. 2017; Messina, Parihar & Distefano 2017).

In this context, Getman, Feigelson & Kuhn (2014b) reported empirical evidence for a spatial gradient of stellar ages within two young rich stellar clusters in the nearest giant molecular cloud, the ONC ionizing the Orion nebula, and NGC 2024 ionizing the Flame Nebula. The result is that stars in cluster cores appear younger (that is, formed later) than stars in cluster peripheries. These findings are independently supported by spatial gradients in the disc fractions of these clusters, and are not related to mass segregation as the analysis is restricted to stars with masses between ∼0.2 and 1.2 M$_\odot$. The result is based on a new estimator of pre-main sequence (PMS) stellar ages derived from X-ray and near-infrared photometry, Age_{JX}, which avoids some of the pitfalls of ages derived from HRDs (Getman et al. 2014a).

⋆ E-mail: gkosta@astro.psu.edu

The observed spatial age gradient is not predicted by simple cluster formation models; a centrally concentrated cloud core would show stars in the core are older, not younger, than in the periphery (Parmentier & Pfalzner 2013). More complex models are needed involving processes of dynamical expansion of older sub-clusters, sub-cluster mergers, and/or resupply of core gas by in-falling filaments (Getman et al. 2014b). Other studies independently indicate that stars in the dense Trapezium core are younger than more dispersed stars in the Orion nebula cluster (O'Dell et al. 2009; Reggiani et al. 2011; Beccari et al. 2017).

The purpose of this study is to extend the search for stellar age gradients from the two Orion cloud clusters in Getman et al. (2014b) to a larger sample of 19 clusters in more distant molecular clouds. Our effort is based on the data sets from two recent X-ray/infrared stellar cluster surveys: Massive Young Star-Forming Complex Study in Infrared and X-ray (MYStIX; Feigelson et al. 2013) and Star Formation in Nearby Clouds (SFiNCs; Getman et al. 2017). MYStIX provides cluster membership catalogues for 20 OB-dominated star-forming regions (SFRs) at distances from 0.4 to 3.6 kpc (Broos et al. 2013). SFiNCs extends the MYStIX effort to a study of 22 generally nearer SFRs, where the stellar clusters are often dominated by a single massive star – typically a late-O or early-B – rather than by numerous O stars in the MYStIX fields. The SFiNCs young stellar object (YSO) and cluster catalogues are available in Getman et al. (2017, 2018). The spatial distribution of stars in these SFRs is complex, and cluster memberships are identified using a maximum likelihood mixture model (Kuhn et al. 2014; Getman et al. 2018).

The result of our search is that core-halo age gradients are present in the vast majority of the analysed clusters: Delayed or continuing star formation in cluster cores is a general phenomenon. The evidence requires that large samples of stars be averaged together because individual stellar Age_{JX} estimates are not accurate. The paper is organized as follows. The age analysis methodology and the cluster samples are reviewed in Section 2. The discovered intracluster age gradients are presented in Section 3, and the implications for cluster formation are discussed in Section 4.

2 SAMPLES AND METHODS

2.1 Cluster samples

Among the 141 MYStIX (Kuhn et al. 2014) and 52 SFiNCs (Getman et al. 2018) clusters that are identified by an objective likelihood-based statistical procedure (Kuhn et al. 2014), we select the ones that : (1) have a simple morphology (a single dense core surrounded by a sparser halo); (2) are relatively isolated (without or with only weak secondary sub-clusters present in their vicinity); 3) and have a relatively high number of stars with available age estimates. A total of 19 clusters, with 2487 Age_{JX} stars, satisfy these criteria.

Table 1 lists the cluster's designation and centre celestial position taken from Kuhn et al. (2014, MYStIX) and Getman et al. (2018, SFiNCs) as well as the distance from the Sun taken from Feigelson et al. (2013, MYStIX) and Getman et al. (2017, SFiNCs). In the case of M 17 and Rosette, the multiple clumpy stellar structures around the primary ionizing clusters identified by Kuhn et al. are combined here into single entities. In the case of Orion, RCW 36, and Be 59, the core and halo structures identified by Kuhn et al. and Getman et al. are treated here as single entities.

Fig. 1 shows the morphology of six clusters; and the full set of panels for the 19 clusters is available in the Supplementary Material. These stellar spatial distributions are presented in the form of an adaptively smoothed projected stellar surface density. The YSO

Table 1. Rich, isolated young star clusters. Column 1: SFR. Column 2: cluster. The cluster's designation is from Kuhn et al. (2014, MYStIX) and Getman et al. (2018, SFiNCs). Columns 3 and 4. celestial coordinates (J2000) for the cluster centre, taken from Kuhn et al. (2014, MYStIX) and Getman et al. (2018, SFiNCs). Column 5. distance from the Sun. The distance values are taken from Feigelson et al. (2013, MYStIX) and Getman et al. (2017, SFiNCs).

Region	Cluster	RA. (deg)	Dec. (deg)	Distance (pc)
(1)	(2)	(3)	(4)	(5)
Eagle nebula	B	274.675 830	−13.784 167	1750
Flame nebula	A	85.427 083	−1.903 806	414
M 17	L	275.124 580	−16.179 444	2000
NGC 1893	B	80.694 167	33.421 389	3600
NGC 6357	F	261.509 170	−34.278 333	1700
Orion nebula	B+C	83.820 000	−5.389 556	414
RCW 36	B	134.863 750	−43.757 222	700
Rosette Nebula	D	97.980 833	4.944 167	1330
W 40	A	277.861 250	−2.094 167	500
Be 59	B	0.562 134	67.418 764	900
Cep A	A	344.073 598	62.030 905	700
Cep OB3b (Cep B)	A	343.446 066	62.596 289	700
Cep C	A	346.441 016	62.502 827	700
GGD 12-15	A	92.710 405	−6.194 814	830
IC 348	B	56.141 167	32.158 825	300
IC 5146	B	328.381 131	47.265 152	800
LkHa 101	A	67.542 392	35.268 025	510
NGC 7160	A	328.443 151	62.585 448	870
SerpensMain	B	277.492 003	1.216 660	415

catalogues of Kuhn et al. (2014) and Getman et al. (2018) serve as the basis for constructing these maps. The maps are constructed using the Voronoi tessellation technique[1] and are presented in units of observed stars per pc^2 (on a logarithmic scale). These adaptive estimates of the surface density are computed using the *R* function *adaptive.density* from the SPATSTAT package (Baddeley, Rubak & Turner 2015). The celestial positions of the surface density peaks are given in Table 1.

The purpose of the maps is to emphasize the presence of relatively compact and dense stellar cores (white and/or red) surrounded by extended and shallower haloes (green). From the core towards periphery, the stellar surface density typically falls by a factor of $\gtrsim$10. The clusters are captured by the MYStIX/SFiNCs surveys at the spatial scales of two to several parsecs.

2.2 Age methods

The stellar ages for the young stars in the MYStIX and SFiNCs sub-clusters were estimated in Getman et al. (2014a, 2017) using the Age_{JX} method of Getman et al. (2014a). Age_{JX} is applicable only to low-mass PMS stars ($M < 1.2$ M$_\odot$ assuming the Siess, Dufour & Forestini 2000 age scale) with reliable measurements of the intrinsic X-ray luminosity and near-infrared JHK_s photometry. The method is based on an empirical X-ray luminosity–mass relation calibrated to well-studied Taurus PMS stars (Telleschi et al. 2007) and to theoretical evolutionary tracks calculated by Siess et al. (2000). X-ray luminosities specify stellar masses; *J*-band luminosities and mass estimates track with PMS evolutionary models, providing stellar ages. While individual Age_{JX} values may be noisy, median ages for

---

[1] Description of the Voronoi tessellation can be found on-line at https://en.wikipedia.org/wiki/Voronoi_diagram.
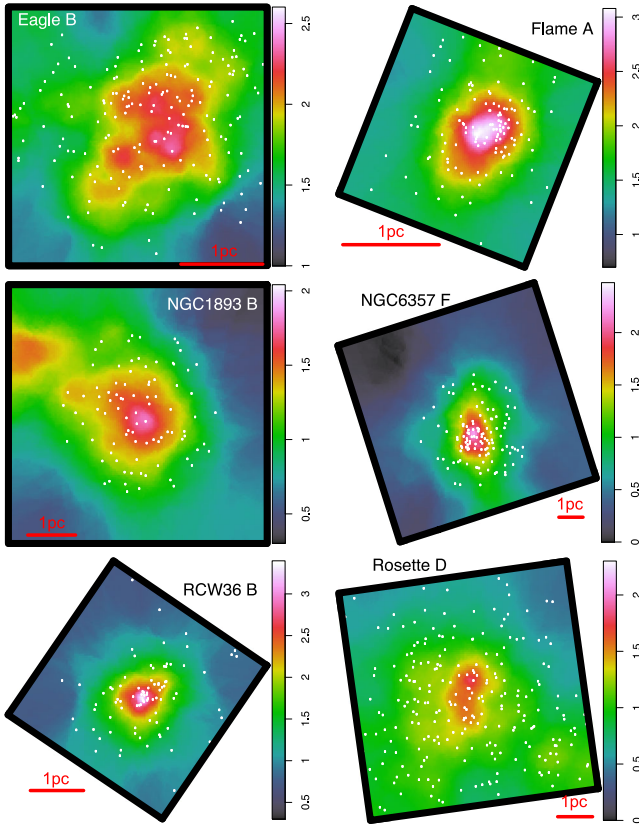
Figure 1. Adaptively smoothed projected stellar surface densities of the clusters with a colour-bar in units of observed stars per pc² (on a logarithmic scale). Six clusters are shown here; similar panels for the full sample of 19 clusters are presented in the Supplementary Materials. The white circles mark the positions of stars with available *Age*$_{JX}$ estimates. The black polygons outline either the original full *Chandra*-ACIS-I fields of view for a single dominant cluster or the cutouts of the *Chandra* fields to separate the cluster of interest from other nearby clusters.

Table 2. *Age*$_{JX}$ Stars. All MYStIX and SFiNCs stars with available age estimates across the 19 clusters of interest. This table is available in its entirety (2487 stars) in the machine-readable form in the online journal. A portion is shown here for guidance regarding its form and content. Column 1: SFR. Column 2: source's IAU designation. This unique source's name keyword can be used to retrieve other numerous X-ray, near-IR, and mid-IR source's properties from the YSO catalogue data sets of Broos et al. (2013, MYStIX) and Getman et al. (2017, SFiNCs). Columns 3 and 4. source's celestial coordinates in decimal degrees (J2000). Column 5. stellar age estimated using the *Age*$_{JX}$ method of Getman et al. (2014a). These age estimates are based on the PMS evolutionary models of Siess et al. (2000).

Region	Source	RA (deg)	Dec. (deg)	*Age*$_{JX}$ (Myr)
(1)	(2)	(3)	(4)	(5)
M17	181959.69-161128.1	274.998713	−16.191166	1.9
M17	182003.75-161339.6	275.015630	−16.227684	3.8
M17	182007.33-161616.0	275.030542	−16.271124	2.2
M17	182007.85-161443.1	275.032725	−16.245325	1.2
M17	182008.08-160938.3	275.033700	−16.160640	0.7
M17	182010.30-161346.1	275.042922	−16.229473	0.2
M17	182010.34-161342.7	275.043122	−16.228539	1.1
M17	182010.92-161036.1	275.045500	−16.176722	0.6
M17	182011.62-161138.3	275.048458	−16.193999	2.4
M17	182012.15-161240.7	275.050630	−16.211330	4.7

similar to that of Baraffe et al. (2015, not shown here in a figure). In contrast, the new generation of magnetic models (Feiden et al. 2015; Feiden 2016) anticipates systematically older ages. Feiden et al. (2015) and Feiden (2016, and references therein) argue for inclusion of magnetic fields, threaded into the stellar interior, in order to mitigate the 'radius inflation' effect, that is an underprediction of stellar radii and overprediction of effective temperatures in low-mass ($M < 1$ M$_\odot$) PMS companions of eclipsing binaries (Kraus et al. 2015) by standard PMS models.

The cluster age gradient analyses reported below in Section 3 are based on the *Age*$_{JX}$ estimates derived using the Siess00 PMS model. In Section 3.3, we comment on the change in the size of these gradients assuming other time-scales, such as MIST and Fieden16M.

The positions of all young stars with available *Age*$_{JX}$ estimates (white points) are superimposed on the smoothed stellar surface density maps (Fig. 1). The positions and ages (based on Siess00) for all these stars (1757 MYStIX and 730 SFiNCs) are also listed in Table 2.

2.3 Statistical Methods

All statistical procedures in this paper were performed using the *R* statistical software environment (R Core Team 2017), including several addon CRAN packages. Relevant functions include: *adaptive.density* in the SPATSTAT package (Baddeley et al. 2015); *ad.test* and *qn.test* in the KSAMPLES package (Scholz & Zhu 2017); *corr.test* in the PSYCH package (Revelle 2017); *cobs* in the COBS package (Ng & Maechler 2007); and *fisher.test* in the STATS package (R Core Team 2017).

3 RESULTS

3.1 Hints of age gradients in individual clusters

For each of the 19 clusters, their stars are separated into four spatially distinct sub-regions requiring that the sub-regions comprise
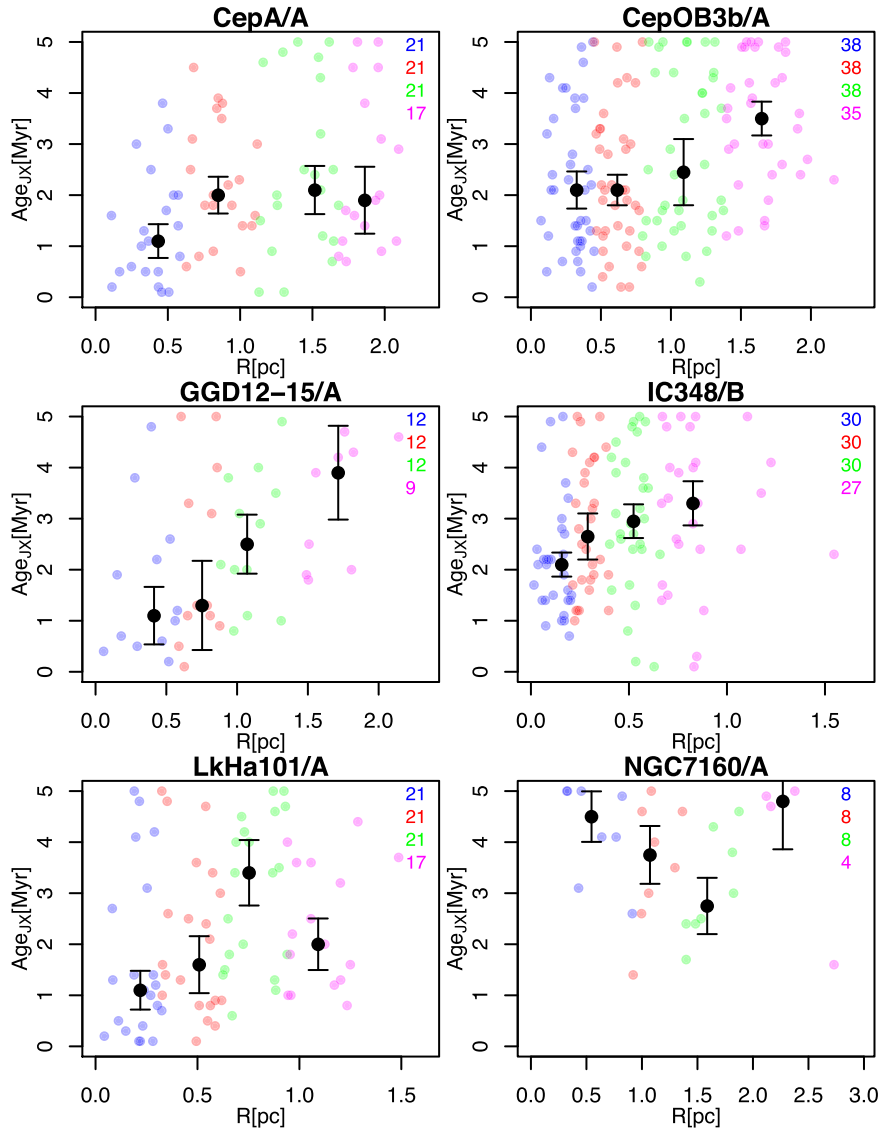
stellar clusters and sub-regions have sufficiently low statistical errors allowing discoveries of spatio-age gradients across the MYStIX SFRs and within the ONC and NGC 2024 clusters (Getman et al. 2014a,b). As most standard PMS age methods, *Age*$_{JX}$ may not provide reliable absolute ages. All sub-region ages derived in this work are relative but are referenced to a uniform time-scale.

Time-scales change with changing an underlying PMS evolutionary model. Here, we consider three different PMS models: The relatively old model of Siess et al. (2000, hereafter Siess00), the new non-magnetic model of Dotter (2016); Choi et al. (2016, hereafter MIST), and the new magnetic model of Feiden, Jones & Chaboyer (2015); Feiden (2016, hereafter Feiden16M). Age transformations among those models can be obtained by placing numerous artificial young stars on the (L_{bol}, T_{eff}) diagram, within the parameter ranges of the SFiNCs/MYStIX *Age*$_{JX}$ stars (see figure in Richert et al. 2017).

The time-scale transformations can be approximated by the following linear functions: $t_{MIST} = -0.45 + 0.83 \times t_{Siess00}$ and $t_{Feiden16M} = -0.31 + 1.67 \times t_{Siess00}$. Compared to Siess00, a newer generation of standard (non-magnetic) evolutionary models, such as MIST, with improved micro-physics (including updated solar abundance scale, linelists, atmospheric convection parameters), predicts systematically younger PMS ages. The MIST time-scale is very

Figure 2. Age analysis within individual stellar clusters. Examples are given for six clusters; the complete sample of 19 clusters is shown in the Supplementary Materials. Panels show Age_{JX} as a function of radial distance from the centres of the clusters for individual Age_{JX} stars. Within each cluster, the stars are divided into four spatially distinct annular sub-regions comprising similar numbers of stars (colour-coded as blue, red, green, and magenta). For each sub-region, its median (Age_{JX}) and 68 per cent CI on the median are marked by a black point and an error bar, respectively. The figure legends provide numbers of plotted stars for each of the four sub-regions.

roughly similar numbers of stars. The Age_{JX} values for individual stars in six exemplifying clusters are shown in Fig. 2, similar figure panels for the full sample of 19 clusters are presented in the Supplementary Materials. For each of the four sub-regions, the median radial distance from the cluster centre, the median age and its 68 per cent confidence interval (CI)[2] are plotted and presented in Table 3. These quantities are labelled as R_1, R_2, R_3, R_4, t_1, t_2, t_3, and t_4. Median distance and age are also calculated for a few blends of

various basic sub-regions, such as the sub-regions '1'+'2', '3'+'4', and '2'+'3'+'4', designated as '1,2', '3,4', and '2,3,4', respectively (Table 3). Also listed in the table are the age differences between the sub-regions '2,3,4' and '1' ($t_{2,3,4} - t_1$) as well as between '3,4' and '1,2' ($t_{3,4} - t_{1,2}$), normalized by the 68 per cent CI. The former age difference emphasizes the age gradient between the very core of the cluster and the remaining stars; whereas, the later difference underlines possible age gradients on relatively larger spatial scales away from the core.

The positive (negative) values of $t_{2,3,4} - t_1$ and $t_{3,4} - t_{1,2}$ indicate trends of increasing (decreasing) age from the cluster centre towards the cluster periphery.

However, for each of the individual clusters, the statistical significance of the observed age variations is generally low. Only a third of the individual cluster age differences exceed twice the 68 per cent

---

[2] The CIs on medians are obtained using the bootstrap re-sampling technique described in Getman et al. (2014a). These are roughly equivalent to $\pm 1\sigma$ intervals, but no assumption of Gaussianity is made. No significance levels can be automatically associated with multiples of these intervals; e.g. $p < 0.003$ for 3σ.

Table 3. Age gradients within individual stellar clusters. Column 1: an SFR harbouring the cluster of interest. Top 9 and bottom 10 SFRs are from the MYStIX and SFiNCs surveys, respectively. Columns 2-5: Numbers of Age_{JX} YSOs (involved in the age gradient analyses) that lie projected against each of the four annular sub-regions around the cluster's centre; with the sub-regions #1 and #4 being the closest and farthest from the centre, respectively. Columns 6–13: median cluster age and median radial distance (from cluster's centre) for the four annular sub-regions. The age errors are 68 per cent CIs on the medians, estimated using the bootstrap re-sampling technique. Columns 14 and 15: median cluster age and median radial distance for the area that combines the sub-regions ##2, 3, and 4 (called as sub-region '2,3,4'). Columns 16 and 17: median cluster age and median radial distance for the area that combines the sub-regions #1 and 2 (called as sub-region '1,2'). Columns 18 and 19: median cluster age and median radial distance for the area that combines the sub-regions #3 and 4 (called as sub-region '3,4'). Columns 20 and 21: age differences (in terms of 68 per cent CIs) between the sub-regions '2,3,4' and '1', and between the sub-regions '3,4' and '1,2'. For instance, the age difference '$t_{2,3,4} - t_1$' is calculated as $(t_{2,3,4} - t_1)/(et_{2,3,4}^2 + et_1^2)^{1/2}$. Positive (negative) differences indicate increasing (decreasing) age from the cluster's core towards the cluster's periphery.

| Region (1)	N_1 (2)	N_2 (3)	N_3 (4)	N_4 (5)	t_1 (Myr) (6)	R_1 (pc) (7)	t_2 (Myr) (8)	R_2 (pc) (9)	t_3 (Myr) (10)	R_3 (pc) (11)	t_4 (Myr) (12)	R_4 (pc) (13)	$t_{2,3,4}$ (Myr) (14)	$R_{2,3,4}$ (pc) (15)	$t_{1,2}$ (Myr) (16)	$R_{1,2}$ (pc) (17)	$t_{3,4}$ (Myr) (18)	$R_{3,4}$ (pc) (19)	$t_{2,3,4} - t_1$ (68 per cent CI) (20)	$t_{3,4} - t_{1,2}$ (68 per cent CI) (21)
Eagle	47	47	47	46	1.50 ± 0.43	0.41	2.30 ± 0.37	0.74	2.10 ± 0.31	1.08	2.15 ± 0.36	1.49	2.10 ± 0.19	1.08	2.10 ± 0.23	0.57	2.10 ± 0.21	1.26	1.28	0.00
Flame	31	31	31	29	0.60 ± 0.17	0.17	1.20 ± 0.26	0.33	1.10 ± 0.29	0.53	1.40 ± 0.28	0.89	1.20 ± 0.15	0.52	0.80 ± 0.13	0.24	1.20 ± 0.18	0.70	2.64	1.79
M 17	106	106	106	105	1.10 ± 0.17	0.52	1.60 ± 0.23	0.99	1.40 ± 0.11	1.53	1.90 ± 0.26	2.73	1.50 ± 0.13	1.53	1.30 ± 0.12	0.73	1.50 ± 0.16	1.93	1.93	1.01
NGC 1893	23	23	23	20	2.70 ± 0.50	0.53	2.60 ± 0.49	0.94	1.80 ± 0.36	1.30	2.90 ± 0.63	1.63	2.25 ± 0.28	1.28	2.65 ± 0.36	0.68	2.20 ± 0.32	1.49	−0.79	−0.93
NGC 6357	30	30	30	29	1.10 ± 0.19	0.39	1.90 ± 0.59	0.77	1.80 ± 0.48	1.40	1.80 ± 0.82	2.07	1.80 ± 0.34	1.39	1.40 ± 0.25	0.59	1.80 ± 0.42	1.82	1.78	0.82
ONC	99	99	99	95	1.50 ± 0.21	0.11	1.80 ± 0.18	0.33	1.90 ± 0.23	0.69	2.00 ± 0.19	0.97	1.90 ± 0.09	0.68	1.60 ± 0.13	0.20	2.00 ± 0.15	0.83	1.73	1.97
RCW 36	22	22	22	19	0.60 ± 0.14	0.14	1.15 ± 0.13	0.50	3.00 ± 0.86	0.83	2.20 ± 0.57	1.48	1.50 ± 0.25	0.80	0.90 ± 0.13	0.38	2.40 ± 0.61	1.09	3.16	2.40
Rosette	60	60	60	58	2.80 ± 0.28	0.92	3.70 ± 0.33	1.76	3.15 ± 0.45	2.51	3.35 ± 0.42	3.38	3.45 ± 0.23	2.48	3.25 ± 0.29	1.34	3.30 ± 0.32	2.97	1.80	0.11
W 40	26	26	26	24	0.60 ± 0.08	0.15	0.80 ± 0.11	0.31	1.20 ± 0.13	0.60	1.75 ± 0.29	1.10	1.15 ± 0.10	0.58	0.70 ± 0.07	0.25	1.25 ± 0.14	0.82	4.17	3.58
Be 59	31	31	31	29	2.20 ± 0.45	0.37	1.50 ± 0.27	0.92	2.40 ± 0.53	1.50	2.10 ± 0.48	1.89	1.90 ± 0.25	1.49	1.80 ± 0.28	0.59	2.30 ± 0.33	1.63	−0.59	1.15
Cep A	21	21	21	17	1.10 ± 0.34	0.43	2.00 ± 0.35	0.85	2.10 ± 0.48	1.52	1.90 ± 0.64	1.86	2.00 ± 0.23	1.40	1.65 ± 0.22	0.61	2.00 ± 0.34	1.65	2.19	0.87
Cep B	38	38	38	35	2.10 ± 0.36	0.33	2.10 ± 0.29	0.62	2.45 ± 0.62	1.09	3.50 ± 0.33	1.65	2.80 ± 0.26	1.07	2.10 ± 0.21	0.45	3.00 ± 0.36	1.36	1.58	2.14
Cep C	10	10	10	7	0.85 ± 0.33	0.46	1.35 ± 0.78	0.76	1.40 ± 0.87	1.27	4.60 ± 1.10	1.73	2.00 ± 0.78	1.06	1.10 ± 0.30	0.65	2.70 ± 1.04	1.46	1.36	1.47
GGD 12-15	12	12	12	9	1.10 ± 0.53	0.41	1.30 ± 0.85	0.75	2.50 ± 0.58	1.07	3.90 ± 0.91	1.71	2.50 ± 0.55	1.02	1.25 ± 0.43	0.58	2.90 ± 0.61	1.31	1.82	2.20
IC 348	30	30	30	27	2.10 ± 0.23	0.16	2.65 ± 0.46	0.29	2.95 ± 0.33	0.52	3.30 ± 0.44	0.83	3.00 ± 0.25	0.52	2.20 ± 0.18	0.21	3.10 ± 0.30	0.63	2.65	2.56
IC 5146	13	13	13	12	2.00 ± 0.67	0.20	1.50 ± 0.13	0.43	2.10 ± 0.50	0.70	2.50 ± 0.78	1.17	1.60 ± 0.25	0.68	1.50 ± 0.18	0.30	2.10 ± 0.46	0.96	−0.56	1.21
LkHa 101	21	21	21	17	1.10 ± 0.33	0.22	1.60 ± 0.56	0.51	3.40 ± 0.65	0.75	2.00 ± 0.48	1.09	2.20 ± 0.38	0.72	1.30 ± 0.30	0.32	2.50 ± 0.56	0.93	2.18	1.89
NGC 7160	8	8	8	4	4.50 ± 0.50	0.55	3.75 ± 0.59	1.07	2.75 ± 0.55	1.59	4.80 ± 0.95	2.27	3.65 ± 0.59	1.44	4.10 ± 0.43	0.92	3.40 ± 0.72	1.82	−1.11	−0.83
Serpens	6	6	6	3	0.45 ± 0.19	0.18	2.05 ± 1.17	0.29	2.30 ± 0.70	0.66	3.90 ± 0.90	1.15	2.40 ± 0.67	0.54	0.75 ± 0.40	0.23	2.40 ± 0.71	0.85	2.79	2.03
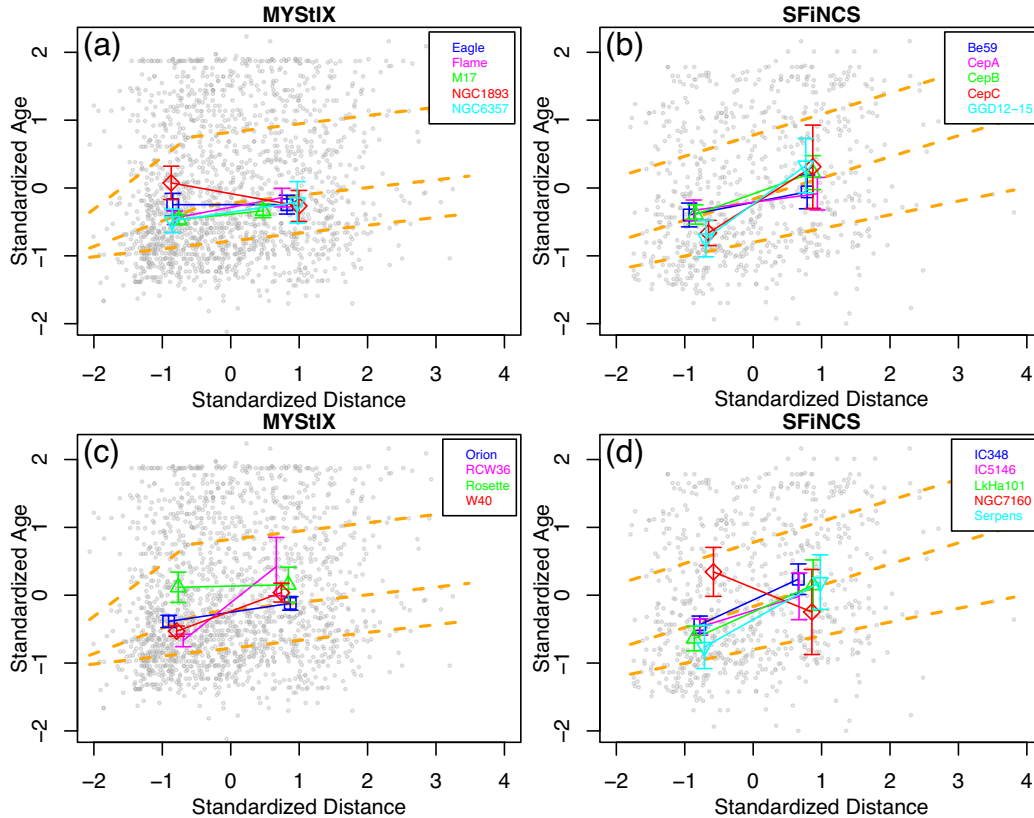
Figure 3. Cluster stacking analysis using standardized variables. Standardized age as a function of standardized radial distance from the cluster centre for all MYStIX clusters (1757 stars as grey points; left-hand panels) and for all SFiNCs clusters (730 stars as grey points; right-hand panels). The dashed orange lines show the relationship of the 25 per cent, 50 per cent (median), and 75 per cent quartiles of age and distance obtained from B-spline regression. The upper and lower panels have the same points and spline fit, and are reproduced to show clearly the age gradients of individual clusters (colored points). The coloured points on panels (a,b,c,d) indicate the $(t_{3,4} - t_{1,2})$ versus $(R_{3,4} - R_{1,2})$ age gradients for individual MYStIX and SFiNCs clusters that were transformed from the physical variables (Table 3) to the standardized variables (see the text).

interval, whereas the remaining age differences are even less significant (Table 3).

Multiple different statistical tests, establishing the existence of an age gradient to high statistical significance, are conducted below to ensure that the results are not method dependent.

Statistical Test 1. For the entire sample of 19 clusters, a random distribution of stellar ages would give a random combination of positive and negative values of $t_{2,3,4} - t_1$ and $t_{3,4} - t_{1,2}$. However, inspection of Table 3 shows a clear dominance of positive values that indicate older ages in the outer regions of the clusters. A total of 15 out of 19 clusters have positive age trends. Bootstrap resampling of the distributions of $t_{2,3,4} - t_1$ and $t_{3,4} - t_{1,2}$ shows that the observed data are inconsistent with a random age distribution at significance levels of $p < 0.009$ and $p < 0.0008$, respectively; i.e. cases of negative $t_{2,3,4} - t_1$ and $t_{3,4} - t_{1,2}$ values for half or more of the clusters in a re-sample are very rare. We therefore find that the collective significance level of a positive age trend in the 19 cluster sample has significance $p < 0.009$.

3.2 Age gradients in merged cluster samples

We can further investigate the presence of an age gradient by erasing the cluster identifier for each star and considering the stars as age indicators in a merged cluster sample. The clusters are merged together into three cluster samples: MYStIX (9 clusters), SFiNCs (10 clusters), and MYStIX+SFINCs (all 19 clusters). We remind

the reader that the MYStIX sample has richer OB dominated clusters, whereas the SFiNCs sample has less-rich clusters typically dominated by single late-O or early-B stars. Since the clusters span wide ranges of ages and spatial extends, the merger is performed using standardized age and radial distance variables.[3] In statistics, standardized variables are used for comparison and stacking of observed scores that were measured on different scales. In our case, for each YSO, its standardized variable (age or radial distance from the cluster centre) is calculated by subtracting the cluster's mean value from a corresponding individual physical observed variable and then dividing the difference by the cluster's 68 per cent CI. For the MYStIX, SFiNCs, and MYStIX+SFINCs cluster samples, their standardized ages as functions of standardized radial distances are shown in Figs 3 and 4. For these merged cluster samples, their standardized quantities, analogous to those given in Table 3, are presented in Table 4.

For the three merged cluster samples, all the three linear regression quartiles[4] (orange lines) in Figs 3 and 4 show clear trends of monotonically increasing age with increasing distance from the cluster centre. Although the median standard age increases by ~1 standard unit from the cluster centre towards the periphery, the

---

[3] See the meaning of the standardized variable at https://en.wikipedia.org/wiki/Standard_score.

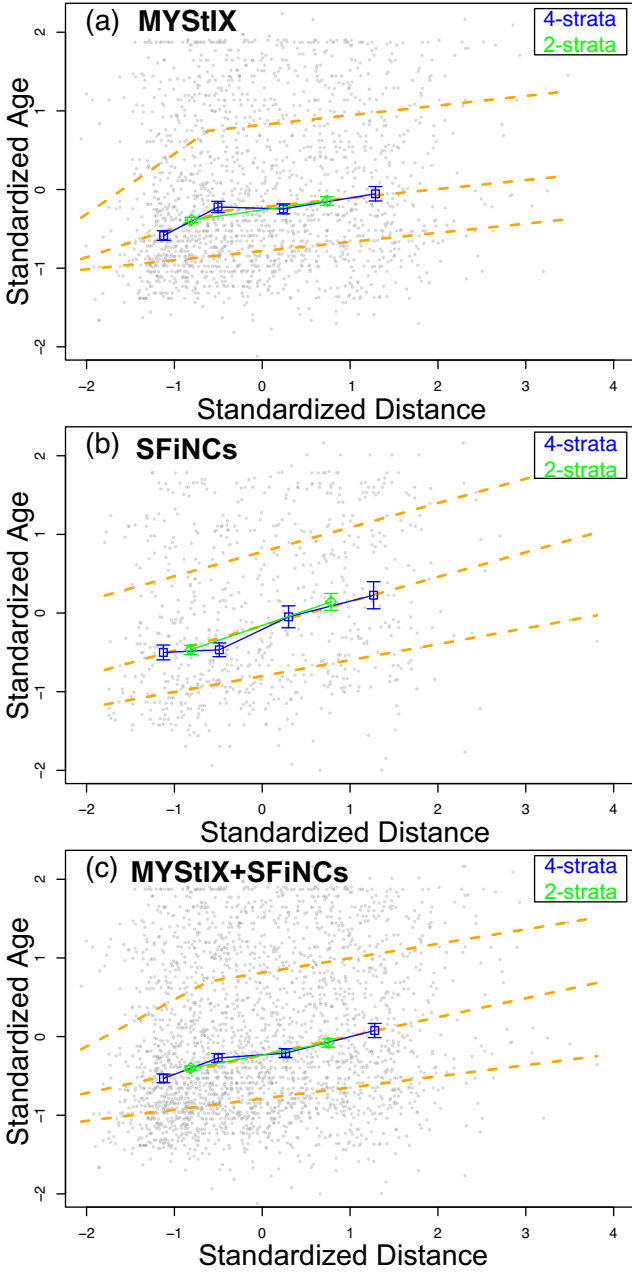[4] The quartile linear regression is performed using the R package COBS.

Figure 4. Cluster stacking analysis using standardized variables. Standardized age as a function of standardized radial distance from the cluster centre for all MYStIX clusters (1757 stars as grey points; panel a), for all SFiNCs clusters (730 stars as grey points; panel b), and for all MYStIX+SFiNCs clusters (2487 stars as grey points; panel c). The dashed orange lines show the relationship of the 25 per cent, 50 per cent (median), and 75 per cent quartiles of age and distance obtained from B-spline regression. The coloured points on panels (a,b,c) indicate the median age versus distance values for the merged MYStIX, SFiNCs, and MYStIX+SFiNCs cluster samples, respectively. These values are given for the two '1,2' and '3,4' strata (green) as well as for the four '1', '2', '3', and '4' strata (blue). These values are tabulated in Table 4 as $(t_{s1,2}, R_{s1,2})$ and $(t_{s3,4}, R_{s3,4})$ (two green strata), and (t_{s1}, R_{s1}), (t_{s2}, R_{s2}), (t_{s3}, R_{s3}) and (t_{s4}, R_{s4}) (four blue strata).

Table 4. Age Gradients For The Merged Cluster Samples (Standardized Variables). Unlike in Table 3, here the age and radial distance from the cluster centre are standardized quantities; thus these are dimensionless quantities (see the text). Column 1: Merged cluster sample. "SFiNCs", "MYStIX", and "MYStIX+SFiNCs" comprise 10, 9, and 19 clusters, respectively. Columns 2-5: Numbers of YSOs (involved in the age gradient analyses) within each of the four annular sub-regions around the cluster's centre; with the sub-regions #1 and #4 being the closest and farthest from the centre, respectively. Columns 6-13: Median cluster age and median radial distance (from cluster's centre) for the four annular sub-regions. The age errors are 68 per cent confidence intervals on the medians, estimated using the bootstrap re-sampling technique. Columns 14-15: Median cluster age and median radial distance for the area that combines the sub-regions "2,3,4" (called as sub-region "2,3,4"). Columns 16-17: Median cluster age and median radial distance for the area that combines the sub-regions ##2, 3, and 4 (called as sub-region "1,2"). Columns 18-19: Median cluster age and median radial distance for the area that combines the sub-regions ##3 and 4 (called as sub-region "3,4"). Columns 20-21: Age differences (in terms of 68 per cent confidence interval) between the sub-regions "2,3,4" and "1", and between the sub-regions "3,4" and "1,2". For instance, the age difference "$t_{s2,3,4} - t_{s1}$" is calculated as $(t_{s2,3,4} - t_{s1})/(e t_{s2,3,4}^2 + e t_{s1}^2)^{1/2}$. Positive (negative) differences indicate increasing (decreasing) age from the cluster's core towards the cluster's periphery.

Sample	N_1	N_2	N_3	N_4	t_{s1}	R_{s1}	t_{s2}	R_{s2}	t_{s3}	R_{s3}	t_{s4}	R_{s4}	$t_{s2,3,4}$	$R_{s2,3,4}$	$t_{s1,2}$	$R_{s1,2}$	$t_{s3,4}$	$R_{s3,4}$	$t_{s2,3,4} - t_{s1}$ (68 per cent CI)	$t_{s3,4} - t_{s1,2}$ (68 per cent CI)
(1)	(2)	(3)	(4)	(5)	(6)	(7)	(8)	(9)	(10)	(11)	(12)	(13)	(14)	(15)	(16)	(17)	(18)	(19)	(20)	(21)
SFiNCs	183	183	183	181	-0.50 ± 0.10	-1.13	-0.47 ± 0.10	-0.49	-0.05 ± 0.14	0.30	0.23 ± 0.16	1.27	-0.08 ± 0.08	0.30	-0.47 ± 0.06	-0.82	0.14 ± 0.10	0.78	3.28	5.15
MYStIX	440	440	440	437	-0.59 ± 0.06	-1.12	-0.22 ± 0.07	-0.50	-0.25 ± 0.06	0.24	-0.05 ± 0.09	1.29	-0.19 ± 0.04	0.24	-0.39 ± 0.03	-0.81	-0.14 ± 0.06	0.74	5.34	3.78
MYStIX + SFiNCs	622	622	622	621	-0.53 ± 0.05	-1.13	-0.27 ± 0.06	-0.50	-0.21 ± 0.06	0.27	0.08 ± 0.09	1.28	-0.14 ± 0.04	0.26	-0.40 ± 0.03	-0.81	-0.08 ± 0.05	0.75	5.74	5.44

interquartile [25 per cent − 75 per cent] range is larger (∼2 standard units), indicating a wide spread of ages about the median (for instance the MYStIX+SFiNCs sample in Fig. 4).

Statistical Test 2. Regardless of the large spread, the Kendall's τ test[5] yields strong statistically significant positive correlations between the standardized age and distance, with the following τ coefficient: $\tau = 0.11$ (MYStIX cluster sample), $\tau = 0.17$ (SFiNCs sample), and $\tau = 0.13$ (MYStIX+SFiNCs sample). In all the cases, the correlations are significant at a level $p \ll 0.0001$.

Statistical Test 3. The Anderson–Darling and Kruskal–Wallis tests independently support these results.[6] These tests are used to evaluate the null hypothesis that the standardized age samples corresponding to different cluster sub-regions come from the same underlying age distribution. For each of the three cluster samples (SFiNCs, MYStIX, and SFiNCs+MYStIX), the tests give tiny probabilities (p-values of $p \ll 0.0001$) that the $t_{s2,3,4}$ and t_{s1} distributions come from a common population (same results are obtained when $t_{s3,4}$ is compared to $t_{s1,2}$).

Statistical Test 4. The inferred inner $(t_{s2,3,4} - t_{s1})$ and outer $(t_{s3,4} - t_{s1,2})$ age differences correspond to $>3.2 \times$CI and $>5.4 \times$CI for the MYStIX/SFiNCs and MYStIX+SFiNCs cluster samples, respectively (Table 4, Fig. 4). The Mood's median test, applied separately to the three cluster samples (SFiNCs, MYStIX, SFiNCs+MYStIX), gives tiny probabilities that the medians of the $t_{s2,3,4}$ versus t_{s1} distributions (or $t_{s3,4}$ versus $t_{s1,2}$ distributions) are identical. The resulting p values are: $p < 0.002$ in the case when $t_{s2,3,4}$ is compared to t_{s1} for the SFiNCs sample; and $p \ll 0.0001$ for the rest of the cases.

Thus, the merged cluster samples show the highly statistically significant age gradients, with stellar ages increasing from the cluster centre towards the periphery.

3.3 Age gradients in physical units

The analyses in Sections 3.1 and 3.2 establish the existence of an age gradient to high statistical significance in several ways. We can now quantify the size of this gradient in physical units of Myr pc^{-1}.

The cumulative distribution functions (c.d.fs.) of the age and the related age gradients are compared between the MYStIX (red) and SFiNCs (green) cluster samples in Fig. 5. Such distributions are also presented for the merged MYStIX+SFiNCs sample (black). In agreement with the results of the previous analyses, the c.d.fs do not pass through the point at (0.0,0.5), indicating that they do not comply with the null hypothesis of having randomly positive and negative age gradients.

Panels (b) and (d) suggest that the SFiNCs clusters tend to have higher age gradient scales (medians of 1.4–1.5 Myr pc^{-1}) than the MYStIX clusters (medians of 0.3–0.7 Myr pc^{-1}). However, this difference is not significant according to an Anderson–Darling test. For the MYStIX versus SFiNCs data sets shown in panels (a), (b), (c), and (d), the p values are 0.16, 0.18, 0.06, and 0.11, respectively.

Considering that the aforementioned MYStIX and SFiNCs distributions do not differ significantly, it is reasonable to combine them together (as MYStIX+SFiNCs; black) to estimate characteristic age gradient scales in our clusters. Figure panels (b) and (d) show that both types of age gradients have similar age gradients of

0.9 Myr pc^{-1} (black curves). This age gradient value is based on the Siess00 time-scale.

According to the time-scale transformations given in Section 2.2, the age gradients based on the MIST and Feiden16M time-scales are expected to be by 17 per cent lower and 67 per cent higher than the ones based on Siess00. So that the typical age gradients are ∼0.75 and 1.5 Myr pc^{-1} assuming the MIST and Feiden16M time-scales, respectively.

4 DISCUSSION

Several years ago, Getman et al. (2014b) discovered that stars in the cluster cores of two nearby young clusters (ONC and Flame) are systematically younger (that is, formed later) than stars in the cluster periphery. In this study, we demonstrate that this property is generally present in young, rich, isolated clusters. A total of 80 percent of the MYStIX and SFiNCs clusters examined here show stellar ages increasing with radial distance from the cluster centre. Although often weak in individual clusters, the collective trend is highly statistically significant. The median amplitude of the age gradients is ∼0.75, 0.9, and 1.5 Myr pc^{-1} when defined on the time-scales of MIST, Siess00, and Feiden16M, respectively.

Other researchers have reported similar age gradients in SFRs (Serpens North, Serpens South, Corona Australis, W 3 Main, and IRAS 19343+2026; references in Getman et al. 2014b). More recently, an independent study of the ONC cluster based on the optical OmegaCAM survey by Beccari et al. (2017) reports the detection of three distinct episodes of star formation. In agreement with our original discovery of the core-halo age gradient in ONC (based on X-ray and infrared data sets of young stars), the optical data of Beccari et al. present evidence for spatio-age gradients in ONC with the younger stellar populations lying projected in a tight concentration within the cluster core and the oldest stellar population more sparsely distributed in and around the core. These results are reminiscent of the spatio-age stellar distributions in ONC previously found in the *HST*-based study by Reggiani et al. (2011). Beccari et al. speculate that the star formation in ONC might have progressed along the line of sight with the youngest population lying further away from the observer. But this explanation requires a particular geometry and cannot account for the presence of age gradients in most young star clusters.

Getman et al. (2014b) provide several plausible scenarios that alone, or in combination with each other, may lead to the observed core-halo age gradients in young stellar clusters. We briefly review these here.

Scenario A is related to the density thresholds in star formation, which would allow the star formation to continue in the cluster core but to cease in the less dense halo. Scenario B invokes the global gravitational contraction and star formation threshold that would lead to the acceleration of star formation rate and formation of younger stars in the denser cloud/cluster core. Scenario C relies on the condition of the late formation of massive stars in the core, accompanied by the formation of some low-mass siblings. Scenario D is based on the kinematic stellar drift in a supervirial cluster and/or stellar ejections by three-body interactions, which would produce an older halo. Scenario E considers the dynamical stellar heating during cluster relaxation as the main source of older halo. Scenarios F and H invoke the merger and expansion of multiple sub-clusters with older sub-cluster populations largely contributing to the halo of the resultant cluster. Scenario G considers the fall of gas filaments

---

[5] The test is performed using the *corr.test* R program from the PSYCH package.
[6] These tests are performed using the *ad.test* and *qn.test* R programs from the KSAMPLES package.
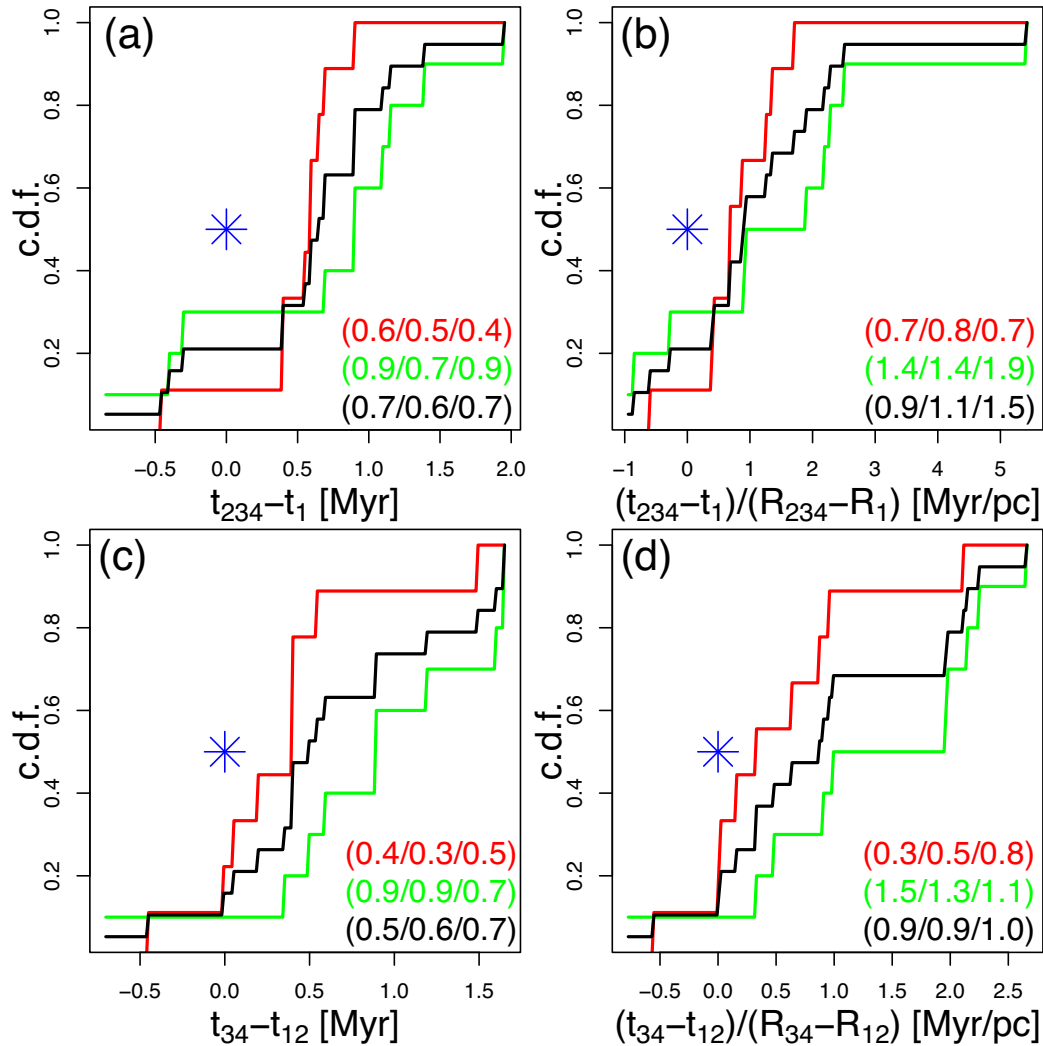
Figure 5. Gradient scales in the MYStIX (red), SFiNCs (green), and MYStIX+SFiNCs (black) cluster samples. (a) Distributions of the age difference between the '2,3,4' and '1' annular sub-regions (see Table 3 for data details). (b) Distributions of the age gradient between the '2,3,4' and '1' annular sub-regions. (c) Distributions of the age difference between the '3,4' and '1,2' annular sub-regions. (d) Distributions of the age gradient between the '3,4' and '1,2' annular sub-regions. The figure legends provide information on the median, mean, and standard deviation of the distributions, in the form of '(median–mean/stdev)'. Had the MYStIX and SFiNCs data complied with the null hypothesis of having randomly positive and negative age gradients, their c.d.f. curves would have passed through the blue star point, at (0.0, 0.5).

into a potential well and further replenishment of the cluster core with younger generations of stars.

Among theoretical astrophysical calculations of star cluster formation, the most promising in explaining the observed age gradients is the global hierarchical collapse (GHC) model by Colín, Vázquez-Semadeni & Gómez (2013) and Vázquez-Semadeni, González-Samaniego & Colín (2017) that leads to a hierarchical assembly of a stellar cluster exhibiting core-halo age gradients. Some of the qualitative star formation scenarios from Getman et al. (2014b), such as B, C, D, F, H, and G, are coherently included in this quantitative model. The GHC model describes a molecular cloud in a free-fall state that globally gravitationally contracts (with a little contribution from turbulence or magnetic field) to form filaments. Relatively small stellar groups form at different times in different locations of the filaments. These stellar groups and gas continue falling towards the centre of the gravitational potential, mixing and replenishing the gas and star material in the central molecular clump that is forming a young stellar cluster. Massive stars tend to form

later within the central clump, at the peak of the star formation rate. The feedback from massive stars cuts off the flow of material from the in-falling filaments, leading to the destruction of the molecular clump and the cessation of star formation in the cluster. Older stars, which formed in multiple in-falling stellar groups prior to reaching the cluster centre, tend to exhibit large velocity dispersions and thus appear further away from the cluster centre at the end of star formation, producing core-halo age gradients.

Similar behaviours of in-falling, star forming filaments are seen in the simulations of Bate (2009, 2012); but these simulations cover only 10^5 yr, which is too short to investigate longer time-scale age gradients seen from the observations of young stellar clusters.

Judging from fig. 9b of Vázquez-Semadeni et al. (2017), the stars in the halo ($r > 0.6$ pc) of their modelled cluster Group-12 have a median age of ~ 2 Myr at a median distance from the cluster centre of $r \sim 1.2$ pc, whereas the stars in the core ($r < 0.6$ pc) have a median age of ~ 1 Myr at a median distance of $r \sim 0.2$ pc; this results in an age gradient of ~ 1 Myr pc^{-1}. This agrees well with the gradient of

0.9 Myr pc^{-1} (based on Siess00) observed in the MYStIX+SFiNCs clusters.

The inferred MYStIX+SFiNCs age gradient of 0.9 Myr pc^{-1} (corresponding to a speed of 0.9 km s^{-1}) also agrees well with the stellar velocity dispersions of $\sim$1 km s^{-1} recently observed in a number of young, nearby, embedded stellar clusters, such as NGC 1333, L 1688, and Chamaeleon I (Foster et al. 2015; Rigliaco et al. 2016; Sacco et al. 2017). Thus, stars drifting away from their site of formation in a dense cloud with a velocity dispersion of $\sim$1 km s^{-1} could also produce the observed core-halo age gradients (our Scenario D above).

The late formation of massive stars in cluster cores has independent evidence. Radial velocity measurements suggest that the 30 M$_\odot$ star θ^1C Ori, which dominates the ONC Trapezium core, is only $\sim$10^4-yr old (O'Dell et al. 2009), and dynamical calculations support this very young age for the Trapezium core (Allen et al. 2017). The embedded cluster W 3 Main has a core with both extremely young and older massive stars (Tieftrunk et al. 1998) surrounded by a larger cluster of older stars (Feigelson & Townsley 2008). Popular scenarios for the formation of massive stars include the quasi-static monolithic collapse model (McKee & Tan 2002) and the dynamical scenarios of either stellar mergers (Bonnell & Bate 2002) or accretion from gas streams, such as the ones present in the aforementioned GHC model (Motte, Bontemps & Louvet 2017; Vázquez-Semadeni et al. 2017). The outcomes of both dynamical scenarios, GHC and stellar mergers, are consistent with the observed late formation of massive stars. According to the latter scenario, some younger more massive stars may have formed through collisions of older less massive stars during the relatively short high-density phase of a cluster core as modelled by Bonnell & Bate (2002). Recall, however, that the age gradient reported here and by Getman et al. (2014b) refers only to lower mass stars (roughly 0.2–1.2 M$_\odot$; based on Siess00 scale) rather than massive stars.

The empirical finding reported in this study – late or continuing formation of stars in the cores of star clusters with older stars dispersed in the outer regions – thus has a strong foundation with other observational studies and with the astrophysical models like the GHC model of Vázquez-Semadeni et al. (2017).

Our study refers to young stellar clusters; all but two (Rosette/D and NGC 7160/A) analysed here clusters have median ages below 3 Myr (based on the Siess00 scale). No positive age trends are detected in NGC 7160/A. The recent *Chandra* study of the rich, isolated NGC 6231 cluster (Kuhn et al. 2017), with the median age above 3 Myr (based on Siess00), finds no a spatial gradient in ages. It is thus possible that such older clusters either 'never had a positive radial age gradient or that a previously existing gradient disappeared with age as a result of dynamical mixing' (Kuhn et al. 2017).

5 CONCLUSIONS

This paper reports the discovery of the core-halo age gradients, with younger cores and older haloes, in the vast majority of the morphologically simple, isolated, and rich MYStIX and SFiNCs clusters. A total of 80 percent of the analysed clusters show upward core-halo age trends (Section 3.1). The collective effect of these trends is highly statistically significant (Section 3.2). Depending on the choice of PMS evolutionary model, the inferred median age gradient within the MYStIX+SFiNCs clusters varies from 0.75 Myr pc^{-1} (based on MIST) to 0.9 Myr pc^{-1} (based on Siess00) to 1.5 Myr pc^{-1} (based on Feiden16M) (Section 3.3). The observed spatio-age gra-

dients can be explained within the framework of the sophisticated astrophysical calculations of star cluster formation such as the GHC model (Section 4).

REFERENCES

Allen C., Costero R., Ruelas-Mayorga A., Sánchez L. J., 2017, MNRAS, 466, 4937
Baddeley A., Rubak E., Turner R., 2015, 'Spatial Point Patterns. Methodology and Applications with R'. Chapman and Hall/CRC
Baraffe I., Homeier D., Allard F., Chabrier G., 2015, A&A, 577, A42
Bate M. R., 2009, MNRAS, 392, 590
Bate M. R., 2012, MNRAS, 419, 3115
Beccari G. et al., 2017, A&A, 604, A22
Bonnell I. A., Bate M. R., 2002, MNRAS, 336, 659
Broos P. S. et al., 2013, ApJS, 209, 32
Choi J., Dotter A., Conroy C., Cantiello M., Paxton B., Johnson B. D., 2016, ApJ, 823, 102
Colín P., Vázquez-Semadeni E., Gómez G. C., 2013, MNRAS, 435, 1701
Da Rio N., Jeffries R. D., Manara C. F., Robberto M., 2014, MNRAS, 439, 3308
Dotter A., 2016, ApJS, 222, 8
Elmegreen B. G., 2000, ApJ, 530, 277
Feiden G. A., 2016, A&A, 593, A99
Feiden G. A., Jones J., Chaboyer B., 2015, in van Belle G., Harris H. C., eds, 18th Cambridge Workshop on Cool Stars, Stellar Systems, and the Sun, Vol. 18. p. 171
Feigelson E. D., Townsley L. K., 2008, ApJ, 673, 354
Feigelson E. D. et al., 2013, ApJS, 209, 26
Foster J. B. et al., 2015, ApJ, 799, 136
Getman K. V. et al., 2014a, ApJ, 787, 108
Getman K. V., Feigelson E. D., Kuhn M. A., 2014b, ApJ, 787, 109
Getman K. V., Broos P. S., Kuhn M. A., Feigelson E. D., Richert A. J. W., Ota Y., Bate M. R., Garmire G. P., 2017, ApJS, 229, 28
Getman K. V., Kuhn M. A., Feigelson E. D., Broos P. S., Bate M. R., Garmire G. P., 2018, MNRAS, in press
Hillenbrand L. A., 1997, AJ, 113, 1733
Huff E. M., Stahler S. W., 2006, ApJ, 644, 355
Jeffries R. D., Littlefair S. P., Naylor T., Mayne N. J., 2011, MNRAS, 418, 1948
Kraus A. L., Cody A. M., Covey K. R., Rizzuto A. C., Mann A. W., Ireland M. J., 2015, ApJ, 807, 3
Krumholz M. R., Tan J. C., 2007, ApJ, 654, 304
Kuhn M. A. et al., 2014, ApJ, 787, 107

Kuhn M. A., Getman K. V., Feigelson E. D., Sills A., Gromadzki M., Medina N., Borissova J., Kurtev R., 2017, AJ, 154, 214

Lada C. J., Lada E. A., 2003, ARA&A, 41, 57

McKee C. F., Tan J. C., 2002, Nature, 416, 59

Messina S., Parihar P., Distefano E., 2017, MNRAS, 468, 931

Motte F., Bontemps S., Louvet F., 2017, preprint (arXiv:1706.00118)

Ng P. T., Maechler M., 2007, 'A Fast and Efficient Implementation of Qualitatively Constrained Quantile Smoothing Splines', Statistical Modelling, Vol. 7, #4, 315. Available at: http://smj.sagepub.com/content/7/4/315.abstract

O'Dell C. R., Henney W. J., Abel N. P., Ferland G. J., Arthur S. J., 2009, AJ, 137, 367

Parmentier G., Pfalzner S., 2013, A&A, 549, A132

Preibisch T., 2012, Res. Astron. Astrophys., 12, 1

R Core Team., 2014, R: A Language and Environment for Statistical Computing. R Foundation for Statistical Computing, Vienna, Austria. Available at: http://www.R-project.org/

Reggiani M., Robberto M., Da Rio N., Meyer M. R., Soderblom D. R., Ricci L., 2011, A&A, 534, A83

Revelle W., 2017, 'Procedures for Psychological, Psychometric, and Personality Research', R package version 1.7.8. Available at: https://CRAN.R-project.org/package=psych

Richert A. J. W., Getman K. V., Feigelson E. D., Kuhn M. A., Broos P. S., Povich M. S., Bate M. R., Garmire G. P., 2017, MNRAS, submitted

Rigliaco E. et al., 2016, A&A, 588, A123

Sacco G. G. et al., 2017, A&A, 601, A97

Scholz F., Zhu A., 2017, 'kSamples: K-Sample Rank Tests and their Combinations', R package version 1.2-7. Available at: https://CRAN.R-project.org/package=kSamples

Siess L., Dufour E., Forestini M., 2000, A&A, 358, 593

Telleschi A., Güdel M., Briggs K. R., Audard M., Palla F., 2007, A&A, 468, 425

Tieftrunk A. R., Megeath S. T., Wilson T. L., Rayner J. T., 1998, A&A, 336, 991

Vázquez-Semadeni E., González-Samaniego A., Colín P., 2017, MNRAS, 467, 1313

Zinnecker H., Yorke H. W., 2007, ARA&A, 45, 481

SUPPORTING INFORMATION

Supplementary data are available at *MNRAS* online.

Figure 1. Adaptively smoothed projected stellar surface densities of the clusters with a colour-bar in units of observed stars per pc^2 (on a logarithmic scale).

Figure 2. Age analysis within individual stellar clusters.

Table 2. *Age$_{JX}$ Stars*. All MYStIX and SFiNCs stars with available age estimates across the 19 clusters of interest.

Please note: Oxford University Press is not responsible for the content or functionality of any supporting materials supplied by the authors. Any queries (other than missing material) should be directed to the corresponding author for the article.

This paper has been typeset from a TeX/LaTeX file prepared by the author.